



Transactions of Nonferrous Metals Society of China

中国有色金属学报(英文版)

ISSN 1003-6326,CN 43-1239/TG

《Transactions of Nonferrous Metals Society of China》网络首发论文

题目: 单晶 Ni_3Al 屈服强度尺寸和应变率综合效应的理论模型(英文)
作者: 张志伟, 蔡微, 王军, 杨荣, 肖攀, 柯孚久, 卢春生
网络首发日期: 2022-04-24
引用格式: 张志伟, 蔡微, 王军, 杨荣, 肖攀, 柯孚久, 卢春生. 单晶 Ni_3Al 屈服强度尺寸和应变率综合效应的理论模型(英文)[J/OL]. Transactions of Nonferrous Metals Society of China.
<https://kns.cnki.net/kcms/detail/43.1239.TG.20220424.1142.014.html>



网络首发: 在编辑部工作流程中, 稿件从录用到出版要经历录用定稿、排版定稿、整期汇编定稿等阶段。录用定稿指内容已经确定, 且通过同行评议、主编终审同意刊用的稿件。排版定稿指录用定稿按照期刊特定版式(包括网络呈现版式)排版后的稿件, 可暂不确定出版年、卷、期和页码。整期汇编定稿指出版年、卷、期、页码均已确定的印刷或数字出版的整期汇编稿件。录用定稿网络首发稿件内容必须符合《出版管理条例》和《期刊出版管理规定》的有关规定; 学术研究成果具有创新性、科学性和先进性, 符合编辑部对刊文的录用要求, 不存在学术不端行为及其他侵权行为; 稿件内容应基本符合国家有关书刊编辑、出版的技术标准, 正确使用和统一规范语言文字、符号、数字、外文字母、法定计量单位及地图标注等。为确保录用定稿网络首发的严肃性, 录用定稿一经发布, 不得修改论文题目、作者、机构名称和学术内容, 只可基于编辑规范进行少量文字的修改。

出版确认: 纸质期刊编辑部通过与《中国学术期刊(光盘版)》电子杂志社有限公司签约, 在《中国学术期刊(网络版)》出版传播平台上创办与纸质期刊内容一致的网络版, 以单篇或整期出版形式, 在印刷出版之前刊发论文的录用定稿、排版定稿、整期汇编定稿。因为《中国学术期刊(网络版)》是国家新闻出版广电总局批准的网络连续型出版物(ISSN 2096-4188, CN 11-6037/Z), 所以签约期刊的网络版上网络首发论文视为正式出版。

Yield strength of monocrystalline Ni₃Al: A theoretical model simultaneously considering the size and strain rate

Zhiwei Zhang ^{a,b}, Wei Cai ^c, Jun Wang ^{a,*}, Rong Yang ^a, Pan Xiao ^a,

Fujiu Ke ^c, Chunsheng Lu ^{d,*}

^a State Key Laboratory of Nonlinear Mechanics (LNM), Institute of Mechanics, Chinese Academy of Sciences, Beijing 100190, China;

^b School of Engineering Science, University of Chinese Academy of Sciences, Beijing 100049, China;

^c School of Physics, Beihang University, Beijing 100191, China;

^d School of Civil and Mechanical Engineering, Curtin University, Perth, WA 6845, Australia

*Corresponding authors: Jun Wang, E-mail: wangjun@lnm.imech.ac.cn, Tel: +86-10-82543930;

Chunsheng Lu, E-mail: c.lu@curtin.edu.au, Tel: +61-8-92664562

Abstract

To comprehensively describe the size and strain rate dependent yield strength of monocrystalline ductile materials, we have established a theoretical model based on the dislocation nucleation mechanism. Taking Ni₃Al as an example, the model first fits results of molecular dynamics simulations to extract material dependent parameters. It then generates a theoretical surface of yield strength, which is finally verified by available experimental data. The model is further checked by available third part molecular dynamics and experimental data of monocrystalline copper and gold. It is shown that this model can successfully leap over the huge spatial and temporal scale gaps between molecular dynamics and experimental conditions to get the reliable mechanical properties of monocrystalline Ni₃Al, copper and gold.

Key words: Yield strength, Size, Strain rate, Monocrystalline, Ni₃Al

1 Introduction

The yield strength of ductile materials such as copper [1], silicon [2], nickel [3] and graphene [4] can be associated with activation of their pre-existing defects such as dislocations. It can also depend on the nucleation of new dislocations in the monocrystalline metals and alloys without pre-existing dislocations. Over recent decades, molecular dynamics (MD) simulations and in-site experiments have been recognized as two effective tools for probing the mechanical properties of metal nanolayered composites [5], high-entropy alloys [6], ceramic composites [7,8], graphene/polymer [9], polycrystalline copper [10], zirconium [11] and titanium alloy [12] materials at the nanoscale. It is shown that the sample size and strain rate effects on yield strength are universal in both the MD simulations [13,14] and experimental tests [15,16]. For example, size and strain rate dependences on the yield strength have been clarified in nanoporous gold [13] and nickel nanowires [14] through MD simulations, and in nanostructured copper [15] and nanocrystalline gold films [16] by experimental tests. However, due to limitation of force and time resolutions, the yield strength of a material with a small size and at an ultra-high strain rate cannot be accurately obtained by experimental measurements. Although this can be filled by numerical techniques such as MD simulations, the size and strain rate that MD simulations deal with are far from that of experiments. Therefore, it is necessary for a theoretical model that can play a bridge to leap over such a spatial and temporal scale gap.

As an intermetallic ordered alloy with the $L1_2$ structure, Ni_3Al has been widely applied in aerospace industries due to its excellent corrosion and creep resistance and high-temperature strength properties [17,18]. Extensive experimental and MD simulation efforts have been made to elucidate the structural and mechanical properties of monocrystalline Ni_3Al . The sample size [19,20] and strain rate [21] effects on yield strength have also been explored. Specifically, Li et al. [19] indicated that the yield strength of dislocation-free Ni_3Al nanocubes increases from ~ 2.10 to ~ 4.50 GPa as the size reduces from ~ 625 to ~ 175 nm, with up to 1 – 2 orders of magnitude higher than that of bulk Ni_3Al [20]. Yu et al. [21] investigated the strain rate effect on deformation mechanism of Ni_3Al . To the best of our knowledge, however, there is still lack of a theoretical model that can comprehensively consider the sample size and strain rate effects on yield strength of Ni_3Al [22,23] and its alloys such as GH4037 [24], 55Ni–23Cr–13Co [25] and Ti–Zr–Cu–Ni–Fe–Co–Mo [26].

Taking the monocrystalline Ni_3Al as an example, we propose a theoretical model in this paper, which can involve the sample size and strain rate effects on yield strength of ductile materials. By using MD simulations, yield strengths of monocrystalline Ni_3Al nanowires were obtained under

various sizes (3 – 12 nm) and strain rates ($5 \times 10^6 \text{ s}^{-1} - 5 \times 10^{10} \text{ s}^{-1}$), which can be applied to verify the theoretical model, together with experimental data under a sample size over 175 nm and at strain rates of $3.2 \times 10^{-3} - 1.1 \times 10^{-2} \text{ s}^{-1}$ [19]. Meanwhile, the nature of sample size and strain rate dependence of yield strength is discussed.

2 Methods

2.1 Potential energy function

An embedded-atom potential function for the Ni-Al system developed by Mishin [27] was taken to describe the atomic interaction in Ni₃Al. In the function, the total energy, U , of a system can be represented as

$$U = \sum_{\substack{i,j \\ i \neq j}} V_{EAM}(r_{ij}) + \sum_i F(\bar{\rho}_i), \quad (1)$$

where the pair potential, $V_{EAM}(r_{ij})$, is a function of the distance r_{ij} between atoms i and j . Moreover, F is the embedding energy of atom i , and $\bar{\rho}_i$ is the electron density, which is written as

$$\bar{\rho}_i = \sum_{i \neq j} g_j(r_{ij}), \quad (2)$$

where $g_j(r_{ij})$ is the electron density of atom j .

Here it is worth noting that such a potential is built up by fitting to data from both experiments and first principles calculations. It can depict an accurate lattice, the mechanical properties, and especially energetics of point defects (vacancies), line defects (dislocations), and planar faults (twin boundaries). It is also essential to study the dislocation nucleation dominated mechanical properties of Ni₃Al [28].

2.2 Simulation details

The monocrystalline Ni₃Al nanowires were created in a cylindrical lateral shape with an aspect ratio of length to diameter (3 – 12 nm) being 3.0. In order to show the changing tendency of yield strength versus the sample size and strain rates, five simulations were performed under each condition. The periodic boundary conditions were introduced in the axial-[111] crystalline directions. Simulations were performed by integrating Newton's equations of motion for all atoms with a time step of 1 fs. At the beginning of simulation, Ni₃Al nanowires were energetically minimized by relaxing a sample for 100 ps at 300 K. To obtain the mechanical properties, a uniaxial

tensile load along the [111] direction was applied with a strain rate ranging from 5.0×10^6 to $5.0 \times 10^{10} \text{ s}^{-1}$. Stress in a stress-strain relationship was calculated by the Virial scheme [29,30]. During uniaxial loading, transverse directions were permitted to relax and remain in a stress-free condition [10,31]. Deformation and defects of Ni_3Al nanowires were recognized by dislocation analysis and then, visualized by the software OVITO [32].

3 Results

As shown in Fig. 1, stress linearly rises with the increase of strain until it reaches the yield strength. Then, a sudden drop of stress occurs as the further increase of strain. The initial configuration of a monocrystalline Ni_3Al nanowire consists of perfect face-centered cubic structure atoms and surface atoms (see left inset in Fig. 1). As strain is less than 7.15% (marked as a blue circle in Fig. 1), there are no dislocations in the Ni_3Al nanowire, implying an elastic deformation. With strain beyond 7.15%, a $1/6[\bar{1}1\bar{2}]$ Shockley dislocation nucleates on the surface of nanowire (see right inset in Fig. 1). Meanwhile, the nanowire yields as stress reaches 16.88 GPa. This indicates that the yield strength of Ni_3Al nanowire is dominated by the nucleation of dislocations.

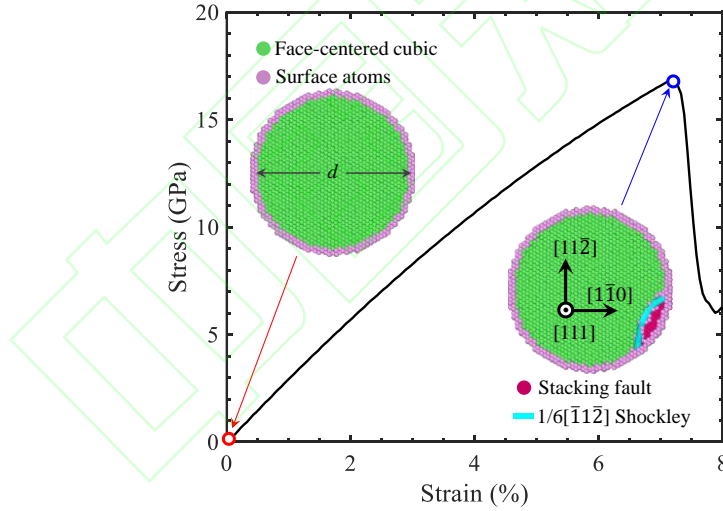


Figure 1. The stress-strain curve of a monocrystalline Ni_3Al nanowire. Insets show snapshots of its cross-section with an initial atomic configuration and a Shockley dislocation nucleating at the yielding point, respectively.

According to Zhu et al. [33], the dislocation nucleation dominated yield strength can be expressed as

$$\sigma = \frac{Q^*}{\Omega} - \frac{k_B T}{\Omega} \ln \frac{k_B T N V_0}{E \epsilon \bar{\Omega}}, \quad (3)$$

where the first term, $Q^*/\bar{\Omega}$, is the athermal nucleation stress with Q and $\bar{\Omega}$ the activation free energy and activation volume. The pre-factor of the second term, $k_B T/\bar{\Omega}$, draws the scale of nucleation stress reduction due to thermal fluctuation, with k_B and T the Boltzmann constant and temperature, respectively. In the logarithmic function, $k_B T N \nu_0$ is the energy exchange rate of candidate nucleation sites with the thermal bath, with ν_0 the attempt frequency and N the number of equivalent surface nucleation sites. $E \dot{\epsilon} \bar{\Omega}$ is the rate of activation energy reduction by the mechanical work, where $\dot{\epsilon}$ and E are the strain rate and Young's modulus.

Here it is worth noting that, due to thermal fluctuation, the ratio of two terms in the logarithmic function in Eq. (3) determines the competition of thermal and mechanical effects in mediating the nucleation stress reduction [33]. At ambient temperature, the number of equivalent surface nucleation points per unit area N is proportional to the surface area of a three-dimensional material as its size changes. Here, the surface area of a nanowire can be expressed as $\pi \cdot d \cdot 3d$ since it has an aspect ratio of length to diameter (d) of 3.0, that is, $N \propto d^2$. Therefore, Eq. (3) can be simplified as

$$\sigma = \sigma_0 - \alpha \ln \frac{A d^2}{\dot{\epsilon}} \quad (4)$$

where σ_0 , α and A are constants because we are interested in the size and strain rate effects. Let us assume that

$$\sigma_0 = \alpha \ln B, \quad (5)$$

where B is a constant dependent on σ_0 and α , Eq. (4) can be rewritten as

$$\sigma = \alpha \ln \frac{B \dot{\epsilon}}{A d^2}. \quad (6)$$

Further, introducing $\beta = B/A$, we have

$$\sigma = \alpha \ln \frac{\beta \dot{\epsilon}}{d^2}. \quad (7)$$

where α and β are the material dependent parameters that can be determined by fitting MD simulation results (see Table 1). In the case of Ni₃Al, they are 0.44 GPa and $1.06 \times 10^{-8} \text{ m}^2 \text{ s}$, respectively. Therefore, Eq. (7) explicitly indicates that the yield strength is dependent on the size and strain rate.

As shown in Fig. 2(a), at a given strain rate of $5 \times 10^8 \text{ s}^{-1}$, as the diameter of a Ni₃Al nanowire increases from 3 to 12 nm, its yield strength decreases from 19.01 to 16.06 GPa, which is well consistent with the theoretical prediction of Eq. (7). In addition, for a Ni₃Al nanowire with the diameter of 6 nm, the yield strength rises from 15.55 to 21.13 GPa as strain rate increases from 5×10^6 to $5 \times 10^{10} \text{ s}^{-1}$ (see Fig. 2(b)). The changing trend is also in accordance with the theoretical

curve. Hence, it is seen that the size and strain rate effects on the yield strength obtained by MD simulations can be well described by the theoretical model.

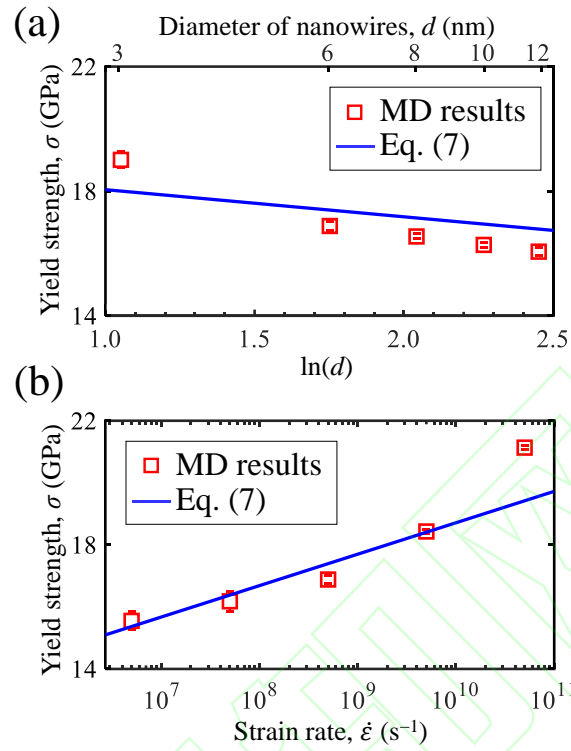


Figure 2. The (a) size and (b) strain rate effects on the yield strength of a Ni_3Al nanowire.

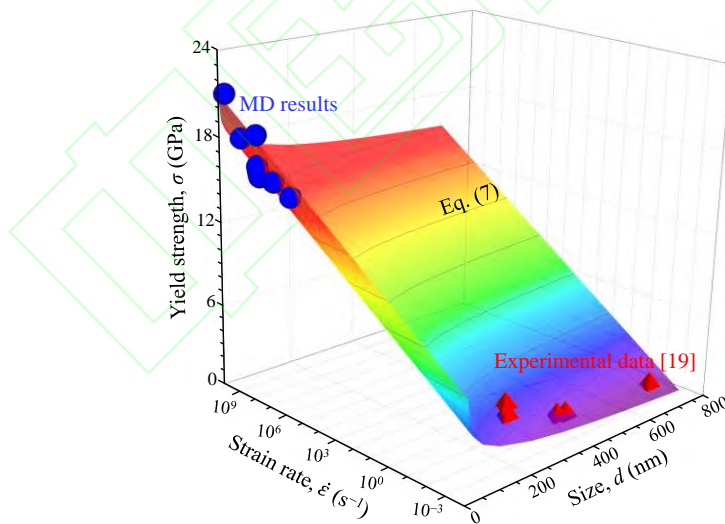


Figure 3. The comprehensive effects of size and strain rate on yield strengths of monocrystalline Ni_3Al samples.

Given that the parameters in Eq. (7) are determined through fitting MD simulation results, a theoretical $\sigma(d, \dot{\epsilon})$ surface can be constructed by extending the size and time scales to that of

experiments. Then, the effectiveness of such a model can be checked by available experimental data. As shown in Fig. 3, the $\sigma(d, \dot{\epsilon})$ surface offers the yield strength of Ni₃Al with a size of 1 – 700 nm under a strain rate of $10^{-3} - 10^{10} \text{ s}^{-1}$. It is obvious that the experimental data from 2.20 – 4.50 GPa (see Table 1) with a strain rate of $3.2 \times 10^{-3} - 1.1 \times 10^{-2} \text{ s}^{-1}$ and a size of 175 – 625 nm [19] are consistent with the theoretical surface. This directly confirms the reliability of the model.

Table 1. The MD and experimental results of yield strengths of single crystal Ni₃Al samples.

	Sample size, d (nm)	Strain rates, $\dot{\epsilon}$ (s ⁻¹)	Yield strength, σ (GPa)
MD	3.0	5.0×10^8	19.01
	6.0	5.0×10^8	16.88
	8.0	5.0×10^8	16.55
	10.0	5.0×10^8	16.27
	12.0	5.0×10^8	16.06
	6.0	5.0×10^6	15.55
	6.0	5.0×10^7	16.18
	6.0	5.0×10^9	18.43
	6.0	5.0×10^{10}	21.13
	Experiment [19]	175	1.1×10^{-2}
180		1.1×10^{-2}	3.75
325		6.2×10^{-3}	2.50
350		5.7×10^{-3}	2.40
625		3.2×10^{-3}	2.20

4 Discussion

As mentioned above, both MD simulations and experiments show that the yield strength of monocrystalline Ni₃Al is related to the nucleation of dislocations, which is depicted in the logarithmic function ($\beta\dot{\epsilon}/d^2$) of Eq. (7). That is, the size and strain rate affect the nucleation of dislocations and thus the yield strength of materials. Specifically, the number of equivalent surface nucleation points (N) increases with the sample size, i.e., $N \propto d^2$. The increasing N lifts the nucleation probability of dislocations from surface nucleation points with a relative lower stress and subsequently leads to the reduction of yield strength. This has been embodied in Eq. (7), as the logarithmic function ($\beta\dot{\epsilon}/d^2$) reduces with the increase of size, resulting in a negative correlation between the yield strength and sample size. Moreover, it is known that the strain rate dependence of

yield strength origins from the competition between the external loading rate and the thermal motion of atoms inside materials, and the yield of materials is related to the processes of atoms crossing the potential barrier to initiate a dislocation [33,34]. Such a competition leads to the raise of yield strength with the increase of external loading rate [34]. This is also reflected in Eq. (7), as the logarithmic function $(\beta\dot{\epsilon}/d^2)$ grows with the increase of strain rate, and thus results in the rise of yield strength. Taking sample size and strain rate effects together, it is seen that the nature of dislocation nucleation dominated yield strength of materials has been captured by our theoretical model. Therefore, it builds a connection between MD and experimental results with the size ranging from 3 to 700 nm (2 orders of magnitude) and the strain rate crossing 13 orders of magnitude from 10^{-3} to 10^{10} s $^{-1}$ for Ni $_3$ Al samples.

The size and strain rate dependent yield strength is also frequently confirmed in other monocrystalline ductile materials such as copper and gold. Specifically, MD simulations reveal that yield strength of copper nanowires decreases with the increase of sample size at a constant strain rate (Table 2) [35]. MD simulations also show that yield strength rises with strain rate as the sample size is fixed (Table 2) [36]. Although similar trend is seen from experimental data as the sample size changes [37], experimental data can hardly compare with MD results since at least 2 orders discrepancy exists at the spatial scale between MD and experimental sizes, let alone the 10 orders temporal gap. Adopting $\alpha = 0.2$ GPa and $\beta = 2.48 \times 10^{-10}$ m 2 s, Eq. (7) well describes the size and strain rate dependent yield strength of monocrystalline copper (Fig. 4(a)). Fig. 4(b) further shows that Eq. (7) with $\alpha = 0.07$ GPa and $\beta = 3.49 \times 10^{-9}$ m 2 s can also connect MD results [38,39] and experimental data [40–42] of monocrystalline gold (Table 3).

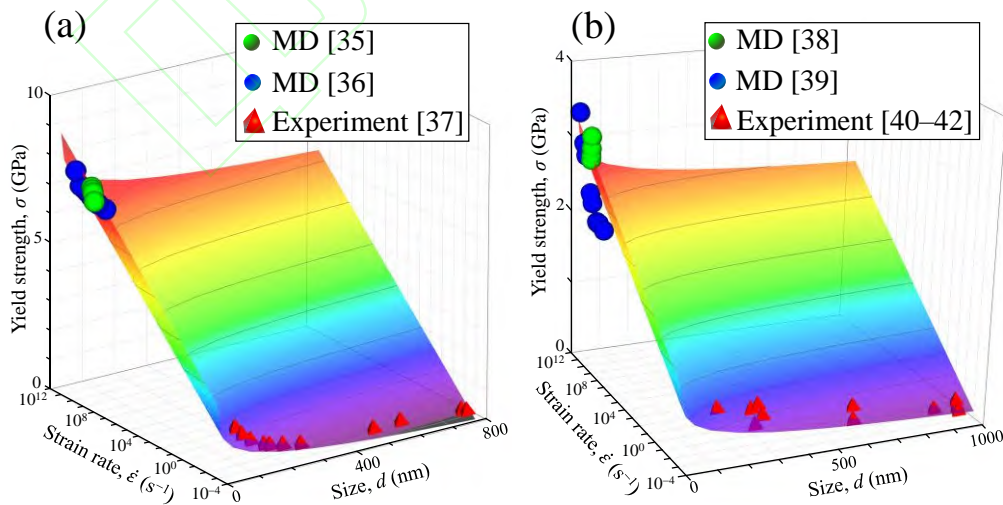


Figure 4. The comprehensive effects of size and strain rate on yield strengths of monocrystalline (a) copper and (b) gold nanowires.

Taking applications of the theoretical model to the size and strain rate dependent yield strength of monocrystalline Ni₃Al, copper and gold together, it is shown that the model can leap over at least 2 orders of spatial and 10 orders of temporal scale gaps between the MD and experimental results of monocrystalline ductile materials such as Ni₃Al, copper and gold to get their reliable mechanical properties. It is also worth noting that the size effect on yield strength of a material is distinct as the sample size is below 1 μm . Moreover, the loading condition with a strain rate below 10^{-3} s^{-1} can be regarded as quasistatic, indicating a negligible variation of yield strength with strain rates below this value. Therefore, the theoretical model applies to spatial scales below 1 μm and temporal scales beyond 10^{-3} s^{-1} .

Table 2. Yield strengths of monocrystalline copper nanowires.

	Sample size, d (nm)	Strain rates, $\dot{\epsilon}$ (s^{-1})	Yield strength, σ (GPa)
MD [35,36]	3.6	2.0×10^8	7.60
	5.4	2.0×10^8	7.50
	7.2	2.0×10^8	7.40
	10.8	2.0×10^8	7.10
	2.0	1.0×10^7	7.11
	2.0	5.0×10^7	7.16
	2.0	1.0×10^8	7.17
	2.0	2.0×10^8	7.28
	2.0	5.0×10^8	7.38
	2.0	1.0×10^9	7.44
	2.0	2.0×10^9	7.47
Experiment [37]	90.0	1.1×10^{-2}	1.25
	108.0	9.3×10^{-3}	0.99
	132.0	7.6×10^{-3}	0.75
	170.0	5.9×10^{-3}	0.53
	223.0	4.5×10^{-3}	0.39
	275.0	3.6×10^{-3}	0.30
	492.0	2.0×10^{-3}	0.27
	573.0	1.7×10^{-3}	0.32
	775.0	1.3×10^{-3}	0.14

Table 3. Yield strengths of monocrystalline gold nanowires.

	Sample size, d (nm)	Strain rates, $\dot{\epsilon}$ (s^{-1})	Yield strength, σ (GPa)
MD [38,39]	3.0	1.9×10^7	2.11
	3.0	9.0×10^7	2.14
	3.0	1.9×10^8	2.14
	3.0	8.6×10^8	2.34
	3.0	1.7×10^9	2.45
	3.0	7.6×10^9	2.90
	3.0	1.5×10^{10}	3.04
	3.0	5.5×10^{10}	3.41
	2.9	1.4×10^9	2.90
	3.9	1.4×10^9	2.95
	5.0	1.4×10^9	3.05
	5.8	1.4×10^9	3.20
	Experiment [40–42]	266.7	7.0×10^{-1}
587.6		3.0×10^{-1}	0.18
951.7		2.0×10^{-1}	0.09
266.7		4.0×10^{-1}	0.57
587.6		4.0×10^{-1}	0.35
951.7		4.0×10^{-1}	0.20
875.1		4.0×10^{-1}	0.13
957.0		4.0×10^{-1}	0.11
148.1		1.4×10^{-2}	0.54
253.4		7.9×10^{-3}	0.49
290.8		6.9×10^{-3}	0.39
454.4		4.4×10^{-3}	0.34

5 Conclusion

In summary, a series of molecular dynamics simulations of monocrystalline Ni₃Al nanowires have been performed under uniaxial tension by considering the various sample sizes and strain rates. The theoretical model has been established by comprehensively considering the sample size and strain rate effects on the dislocation nucleation dominated yield strength of ductile materials. The main conclusions can be summarized as follows:

- (1) The model well describes the MD simulation results (15.55 – 21.13 GPa) with sample sizes of 3 – 12 nm at strain rates of 5×10^6 to $5 \times 10^{10} s^{-1}$ and experimental data (2.20 – 4.50 GPa) with the sample size ranging from 175 to 625 nm and strain rates of 3.2×10^{-3} to $1.1 \times 10^{-2} s^{-1}$.

- (2) The theoretical model can also be applied to leap over spatial and temporal scale gaps between the MD and experimental results of face-centered cubic metallic materials such as copper and gold nanowires.

It is expected that these findings could provide means for analyzing the size and strain rate dependent yield strength of ductile materials.

Acknowledgement

This work has been supported by the National Natural Science Foundation of China (Grant Nos. 11772332, 11790292 and 11727803), the NSFC Basic Science Center Program for “Multiscale Problems in Nonlinear Mechanics” (Grant No. 11988102), the Strategic Priority Research Program of the Chinese Academy of Sciences (Project No. XDB22040501), and the Opening Fund of State Key Laboratory of Nonlinear Mechanics. The simulations were performed on resources provided by the ScGrid of Supercomputing Center, Computer Network Information Center of the Chinese Academy of Sciences, the LNMGrid of the State Key Laboratory of Nonlinear Mechanics, and the Pawsey Supercomputing Center with funding from the Australian Government and the Government of Western Australia.

References

- [1] SHISHVAN S S, van der GIESSEN E. Distribution of dislocation source length and the size dependent yield strength in freestanding thin films [J]. *Journal of the Mechanics and Physics of Solids*, 2010, 58: 678–695.
- [2] SHUANG F, AIFANTIS K E. A first molecular dynamics study for modeling the microstructure and mechanical behavior of Si nanopillars during lithiation [J]. *ACS Applied Materials & Interfaces*, 2021, 13: 21310–21319.
- [3] SHUANG F, DAI Z H, AIFANTIS K E. Strengthening in metal/graphene composites: capturing the transition from interface to precipitate hardening [J]. *ACS Applied Materials & Interfaces*, 2021, 12: 26610–26620.
- [4] SHI X H, PENG B, PUGNO N M, GAO H J. Stretch-induced Softening of Bending Rigidity in Graphene [J]. *Applied Physics Letters*, 2012, 100: 191913.
- [5] WANG Y D, LI J J. Strengthening Cu/Ni nanolayered composites by introducing thin Ag interlayers: A molecular dynamics simulation study [J]. *Journal of Applied Physics*, 2021, 130: 045109.

- [6] LU W J, LI J J. Synergetic deformation mechanism in hierarchical twinned high-entropy alloys [J]. *Journal of Materials Science & Technology*, 2021, 102: 80–88.
- [7] LI X W, SHI T, LI B, CHEN X C, ZHANG C W, GUO Z G, ZHANG Q X. Subtractive manufacturing of stable hierarchical micro-nano structures on AA5052 sheet with enhanced water repellence and durable corrosion resistance [J]. *Materials & Design*, 2019, 183: 108152.
- [8] LI X W, LIANG J S, SHI T, YANG D N, CHEN X C, ZHANG C W, LIU Z H, LIU D Z, ZHANG Q X. Tribological behaviors of vacuum hot-pressed ceramic composites with enhanced cyclic oxidation and corrosion resistance [J]. *Ceramics International*, 2020, 46: 12911–12920.
- [9] DAI Z H, WANG G R, LIU L Q, HOU Y, WEI Y G, ZHANG Z. Mechanical behavior and properties of hydrogen bonded graphene/polymer nano-interfaces [J]. *Composites Science and Technology*, 2016 136: 1–9.
- [10] ZHANG Y Q, JIANG S Y. Molecular dynamics simulation on mechanisms of plastic anisotropy in nanotwinned polycrystalline copper with {111} texture during tensile deformation [J]. *Transactions of Nonferrous Metals Society of China*, 2021, 31: 1381–1396.
- [11] Tang X Z, Zhang H S, Guo Y F. Atomistic simulations of interactions between screw dislocation and twin boundaries in zirconium [J]. *Transactions of Nonferrous Metals Society of China*, 2018, 28: 1192–1199.
- [12] Cui S W, Shi Y H, Zhang C S. Microstructure and mechanical properties of TC4 titanium alloy K-TIG welded joints [J]. *Transactions of Nonferrous Metals Society of China*, 2021, 31: 416–425.
- [13] VOYIADJIS G Z, SAFFARINI M H, RUESTES C J. Characterization of the strain rate effect under uniaxial loading for nanoporous gold [J]. *Computational Materials Science*, 2021, 194: 110425.
- [14] HUANG D, ZHANG Q, QIAO P Z. Molecular dynamics evaluation of strain rate and size effects on mechanical properties of FCC nickel nanowires [J]. *Computational Materials Science*, 2011, 50: 903–910.
- [15] WANG Y M, MA E. Temperature and strain rate effects on the strength and ductility of nanostructured copper [J]. *Applied Physics Letters*, 2003, 83: 3165–3167.
- [16] CHASIOTIS I, BATESON C, TIMPANO K, MCCARTY A S, BARKER N S, STANEC J R. Strain rate effects on the mechanical behavior of nanocrystalline Au films [J]. *Thin Solid Films*, 2007, 515: 3183–3189.
- [17] ZHANG Z W, FU Q, WANG J, XIAO P, KE F J, LU C S. Hardening Ni₃Al via complex

- stacking faults and twinning boundary [J]. *Computational Materials Science*, 2021, 188: 110201.
- [18]ZHANG Z W, FU Q, WANG J, YANG R, XIAO P, KE F J, Lu C S. Simultaneously achieving strength and ductility in Ni₃Al nanowires with superlattice intrinsic stacking faults [J]. *International Journal of Mechanical Sciences*, 2022, 215: 106953.
- [19]LI P, WANG X G, ZHOU Y Z, PFETZING-MICKLICH J, SOMSEN C, EGGELER G. Effect of aspect ratio on the deformation behavior of dislocation-free Ni₃Al nanocubes [J]. *Nanomaterials*, 2020, 10: 2230.
- [20]UCHIC M D, DIMIDUK D M, FLORANDO J N, NIX W D. Sample dimension influence strength and crystal plasticity [J]. *Science*, 2004, 305: 986–989.
- [21]YU H F, JONES I P, SMALLMAN R E. The effects of temperature, composition and strain rate on the deformation microstructure of Ni₃Al [J]. *Philosophical Magazine A*, 1994, 71: 951–967.
- [22]XUE H, ZHAO J Q, LIU Y K, ZHANG C X, LUO J T, δ -phase precipitation regularity of cold-rolled fine-grained GH4169 alloy plate and its effect on mechanical properties[J]. *Transactions of Nonferrous Metals Society of China*, 2020, 30: 3287–3295.
- [23]YI Z, XU Y L, PENG P, CHEN J H, Impact of replacement of Re by W on dislocation slip mediated creeps of γ' -Ni₃Al phases[J]. *Transactions of Nonferrous Metals Society of China*, 2021, 31: 2013–2023.
- [24]JIANG J F, XIAO G F, WANG Y, LIU Y Z, ZHANG Y, High temperature deformation behavior and microstructure evolution of wrought nickel-based superalloy GH4037 in solid and semi-solid states[J]. *Transactions of Nonferrous Metals Society of China*, 2020, 30: 710–726.
- [25]WANG K M, JING H Y, XU L Y, ZHAO L, HAN Y D, LI H Z, SONG K, Microstructure evolution of 55Ni–23Cr–13Co nickel-based superalloy during high-temperature cyclic deformation[J]. *Transactions of Nonferrous Metals Society of China*, 2021, 31: 3452–3468.
- [26]LI L, ZHAO W, FENG Z X, SUN J, LI X Q, Microstructure and shear strength of γ -TiAl/GH536 joints brazed with Ti–Zr–Cu–Ni–Fe–Co–Mo filler alloy[J]. *Transactions of Nonferrous Metals Society of China*, 2020, 30: 2143–2155.
- [27]MISHIN Y. Atomistic modeling of the γ and γ' -phases of the Ni–Al system [J]. *Acta Materialia*, 2004, 52: 1451–1467.
- [28]AMODEO J, BEGAU C, BITZEK E. Atomistic simulations of compression tests on Ni₃Al nanocubes [J]. *Materials Research Letters*, 2014, 2: 140–145.
- [29]DENG X Z, LANG L, MO Y F, DONG K J, TIAN Z, HU W Y, Solid-solid phase transition of tungsten induced by high pressure: A molecular dynamics simulation[J]. *Transactions of*

Nonferrous Metals Society of China, 2021, 30: 2980–2993.

- [30] WU H, XU F, REN J Y, LAN X D, YIN Y, LIANG L X, SONG M, LIU Y, LI J, LI Q X, HUANG W D, Rate-dependent inhomogeneous creep behavior in metallic glasses[J]. Transactions of Nonferrous Metals Society of China, 2021, 31: 1758–1765.
- [31] WANG J, QIN J Y, ZHOU J X, CHENG K M, ZHAN C W, ZHANG S Q, LI X X, SHEN K C, ZHOU Y, Correlation between mixing enthalpy and structural order in liquid Mg–Si system[J]. Transactions of Nonferrous Metals Society of China, 2021, 31: 853–864.
- [32] STUKOWSKI A, Visualization and analysis of atomistic simulation data with OVITO—the Open Visualization Tool [J]. Modelling and Simulation in Materials Science and Engineering, 2009, 18: 015012.
- [33] ZHU T, LI J, SAMANTA A, LEACH A, GALL K. Temperature and strain-rate dependence of surface dislocation nucleation [J]. Physical Review Letters, 2008, 100: 025502.
- [34] XIAO P, WANG J, YANG R, KE F J, BAI Y L. Transition of mechanisms underlying the rate effects and its significance [J]. Computational Materials Science, 2015, 98: 70–75.
- [35] CAO H, RUI Z Y, YANG F Q. Mechanical properties of Cu nanowires: Effects of cross-sectional area and temperature [J]. Materials Science and Engineering: A, 2020, 791: 139644.
- [36] WU H A. Molecular dynamics study of the mechanics of metal nanowires at finite temperature. [J]. European Journal of Mechanics - A/Solids, 2006, 25: 370–377.
- [37] KIENER D, HOSEMANN P, MALOY S A, MINOR A M. In situ nanocompression testing of irradiated copper [J]. Nature materials, 2011, 10: 608–613.
- [38] JU, S P, LIN J S, LEE W J, A molecular dynamics study of the tensile behaviour of ultrathin gold nanowires [J]. Nanotechnology, 2004, 15: 1221–1225.
- [39] WANG W, YI C, MA B, Molecular dynamics simulation on the tensile behavior of gold nanowires with diameters between 3 and 6 nm [J]. Proceedings of the Institution of Mechanical Engineers, Part N: Journal of Nanoengineering and Nanosystems, 2013, 227: 135–141.
- [40] KIM J Y, GREER J R, Tensile and compressive behavior of gold and molybdenum single crystals at the nano-scale[J]. Acta Materialia, 2009, 57: 5245–5253.
- [41] GREER J, OLIVER W, NIX W, Size dependence of mechanical properties of gold at the micron scale in the absence of strain gradients[J]. Acta Materialia, 2005, 53: 1821–1830.
- [42] LEE S W, HAN S M, NIX W D, Uniaxial compression of fcc Au nanopillars on an MgO substrate: the effects of prestraining and annealing[J]. Acta Materialia, 2009, 57: 4404–4415.

单晶 Ni_3Al 屈服强度尺寸和应变率综合效应的理论模型

张志伟^{a,b}, 蔡微^c, 王军^{a,*}, 杨荣^a, 肖攀^a, 柯孚久^c, 卢春生^{d,*}

^a 中国科学院力学研究所 非线性力学国家重点实验室, 北京 100190

^b 中国科学院大学 工程科学学院, 北京 100049

^c 北京航空航天大学 物理学院, 北京 100191

^d School of Civil and Mechanical Engineering, Curtin University, Perth, WA 6845, Australia

* 通讯作者: wangjun@lnm.imech.ac.cn, 王军, (86)-10-82543930

c.lu@curtin.edu.au, 卢春生, (61)-8-92664562

摘要: 为了综合考虑尺寸和应变率效应对单晶延性材料屈服强度的影响, 我们建立了一个基于位错形核机制的理论模型。采用 Ni_3Al 为例, 该模型首先通过分子动力学模拟结果拟合出材料参数。然后, 通过材料参数构建屈服强度的理论曲面。最后用现有实验数据检验理论模型。该模型也通过现有第三方的单晶铜和金的分子动力学和实验数据做了检验。结果表明该模型可以跨越分子动力学和实验条件之间巨大的空间和时间差异, 从而得到单晶 Ni_3Al , 铜和金的可信赖的力学性能。

关键词: 屈服强度; 尺寸; 应变率; 单晶; Ni_3Al